catalysts

MDPI

Article

Application of Deep Eutectic Solvents (DES) for the Synthesis of Iron Heterogeneous Catalyst: Application to Sulfamethoxazole Degradation by Advanced Oxidation Processes

Antón Puga, Emilio Rosales, Marta Pazos and María Angeles Sanromán *

Grupo de Bioingeniería y Procesos Sostenibles, CINTECX, Universidade de Vigo, Campus Lagoas-Marcosende, 36310 Vigo, Spain; apuga@uvigo.es (A.P.); emiliorv@uvigo.es (E.R.); mcurras@uvigo.es (M.P.)
* Correspondence: sanroman@uvigo.es

Abstract: The development of novel approaches to the remotion of pharmaceuticals in wastewater is a subject of concern due to their effect on living beings and the environment. Advanced oxidation processes and the use of relevant catalysts are feasible treatment alternatives that require further development. The development of suitable heterogeneous catalysts is a necessity. This work proposes the synthesis of an iron catalyst in a deep eutectic solvent (Fe-DES) composed of choline chloride and citric acid, which was physically and chemically characterized using SEM-EDS and TEM, FTIR, RAMAN, XRD and XPS. The characterisation confirmed the presence of iron in the form of hematite. Fe-DES was shown to be a multipurpose catalyst that can be applied in the removal of sulfamethoxazole as a reagent in the Fenton and electro-Fenton processes and as an activator of peroxymonosulfate (PMS) processes. After testing the catalyst with the aforementioned techniques, the best result was achieved by combining these processes in an electro-PMS, with great efficiency achieved by dual activation of the PMS with the catalyst and electric field, attaining total elimination at natural pH in 90 min. Furthermore, the degradation was confirmed by the detection of short-chain carboxylic acids (oxalic, succinic, and acetic) and reduction in toxicity values. These results confirm the suitability of Fe-DES to degrade high-priority pharmaceutical compounds.

Keywords: sulfamethoxazole; DES-based catalyst; PLA electrodes; hydroxyl radical; sulfate radical

Citation: Puga, A.; Rosales, E.; Pazos, M.; Sanromán, M.A. Application of Deep Eutectic Solvents (DES) for the Synthesis of Iron Heterogeneous Catalyst: Application to Sulfamethoxazole Degradation by Advanced Oxidation Processes. *Catalysts* **2023**, *13*, 679. https://doi.org/10.3390/catal13040679

Academic Editors: Enric Brillas, Filippo Perna and Antonio Zuorro

Received: 26 January 2023
Revised: 2 March 2023
Accepted: 28 March 2023
Published: 30 March 2023

1. Introduction

Advanced oxidation processes (AOPs) have become one of the most widely used treatments to decontaminate wastewater, with great effectiveness in removing organic pollutants [1]. Amongst the different AOPs, the application of an electric field causes a very positive synergistic effect, making electrochemical advanced oxidation processes (EAOPs) especially attractive treatments [2,3]. These processes generate different reactive species capable of degrading recalcitrant organic pollutants, in turn eliminating other problems derived from them, such as antibiotic [4] and bacterial resistance [5].

EAOPs can vary greatly depending on the species that are formed in the process. However, many of the key factors in the treatments are common, regardless of the specific treatment type and oxidising species used to remove pollutants [2]. The electrode materials, the density or current potential used, and the electrolyte (concentration, type) can make EAOP treatment very effective and environmentally friendly [6]. The electrode materials used are one of the bottlenecks for EAOPs [7]. The current density or potential is another important factor that needs to be taken into account and is directly related to the electrode material. With a conductive electrode, it is not necessary to apply an excessive current potential, making the treatment more economical and cost-effective [8]. Finally, the selection of an appropriate electrolyte for the process, as well as in suitable concentration, can

increase the effectiveness of the process by enhancing conductivity [9]. These three factors are limiting and, therefore, many of the efforts by researchers in recent years have been based on optimising these factors.

Regarding the most used oxidative species, the hydroxyl radical ($HO^{\bullet}$, potential redox of 2.8 V vs. SHE) and the sulfate radical ($SO_4^{\bullet -}$, potential redox of 2.5–3.1 V vs. SHE) stand out above the others as fast and effective oxidising species in the decontamination of wastewater with organic contaminants [10]. The radical $HO^{\bullet}$ is generated by the Fenton reaction, obtained by the catalytic decomposition of hydrogen peroxide that takes place in the presence of iron according to Equation (1).

$$Fe^{2+} + H_2O_2 \rightarrow Fe^{3+} + HO^{\bullet} + OH^- \quad (1)$$

For its part, the radical is generated from peroxymonosulfate (PMS, -O_3S-O-O-H), also known by the commercial name Peroxone® [11]. The sulfate radical has, in addition to a greater redox potential, a longer half-life, which is estimated to be between 30–40 µs (compared to 10^{-3} µs for the hydroxyl radical). For greater efficiency, the PMS can be activated in various ways. The most common involve use of transition metals, such as cobalt (Equation (2)) or iron (Equation (3)), or energy, such as ultraviolet light (Equation (4)), ultrasound (Equation (5)) or electric current (Equation (6)).

$$Co^{2+} + HSO_5^- \rightarrow Co^{3+} + OH^- + SO_4^{\bullet -} \quad (2)$$

$$Fe^{2+} + HSO_5^- \rightarrow Fe^{3+} + OH^- + SO_4^{\bullet -} \quad (3)$$

$$h\nu + HSO_5^- \rightarrow HO^{\bullet} + SO_4^{\bullet -} \quad (4)$$

$$))) + HSO_5^- \rightarrow HO^{\bullet} + SO_4^{\bullet -} \quad (5)$$

$$e^- + HSO_5^- \rightarrow OH^- + SO_4^{\bullet -} \quad (6)$$

In both techniques, the catalyst plays an important role, either as a fundamental part of the process (that is, acting as a reagent) to produce hydroxyl radicals (Fenton), or as a PMS activator if a transition metal is intended to be used, such as iron. This catalyst/activator should be subject to the same principles of economy and ecology as the other three factors mentioned above. Because of this, there has been a trend to find heterogeneous catalysts in order to allow them to be recovered after the process has been completed. In addition, a good heterogeneous catalyst can be reused, complying with the sustainability principles of the circular economy [12]. A wide variety of catalysts of different origins have been tested in recent years: from minerals naturally containing metals [13], to minerals with metals introduced artificially [14], and pyrolyzed materials of vegetable origin, such as biochars, which have also been used as catalysts, containing either naturally occurring [15] or artificially introduced metals [16]. Very recently, deep eutectic solvents (DESs) have emerged as ecological solvents with valuable properties, among which are high thermal stability, excellent ionic conduction, non-toxicity, accessibility and low price, and which are able to be applied at large scales for many applications [17–20]. They have been suggested as a substitute for ionic liquids and volatile organic solvents. In addition, they are beginning to be used for catalysis. Although more research is needed in this field, the application of DESs for the shape-controlled synthesis of metal nanoparticles has had a great impact on the search for and further development of promising electrocatalysts [21]. Dlugosz [22] discussed the physicochemical properties of DES for obtaining functional nanomaterials, including salts, metal oxides, and metals. In this work, the role of DES is considered as a novel means to obtain a wide range of inorganic nanoparticles, whose advantages over traditional production methods lie in energy savings and the in situ functionalisation of

nanoparticles. Gontrani et al. [23] also considered the "template effect" of using DES as inherently highly tunable materials for the preparation of nanomaterials and composites. Specifically, they used DES in the synthesis of zinc-containing nanoparticles, describing three types of synthesis.

In this work, all the treatments considered involve the use of a DES-based heterogeneous catalyst, synthesized from choline chloride and citric acid. The Fenton and PMS processes are tested in two variants: a simple variant (Fenton and PMS activated with iron: A-PMS) and an electrochemical variant, through the well-known electro-Fenton (E-F) and electro-PMS (E-PMS) processes. These are used for the elimination of the antibiotic sulfamethoxazole (SMX), which is part of the Watch List of the European Union as a priority pollutant for investigation. In the case of E-PMS, this involves a combination of electrical current and iron, since the catalyst remains in contact with the solution. As a result, the system proposed consists of a combination of A-PMS and E-PMS, referred to as activated electro-PMS (A-E-PMS), which makes this work innovative, fusing both techniques, which are often used independently. The combination of both activation processes can lead to the formation of two types of radicals: sulfate and hydroxyl, as expressed by Equation (7).

$$Fe^{2+} + e^{-} + HSO_5^{-} \rightarrow Fe^{3+} + HO^{\bullet} + SO_4^{\bullet -} \quad (7)$$

To achieve the most economical treatment possible, the electrodes used in this work were obtained by 3D impression using conductive polylactic acid (PLA). This material is increasingly advocated as a candidate to replace the consumption of plastic of petrochemical origin and already has many applications in the field of electrodes [24,25].

The aim of this work was the removal of SMX with PLA electrodes and a novel DES-based heterogeneous iron catalyst (Fe-DES) for Fenton-like processes, which also served as a PMS activator. This catalyst was extensively characterized (e.g., by FTIR, RAMAN, XRD, XPS, SEM-EDS, TEM). Monitoring of the elimination was carried out using the carboxylic acids generated throughout the process, which were identified and quantified in order to study the degree of mineralisation achieved with these processes. Finally, a toxicity test was carried out to validate the process and determine its final toxicity, comparing the initial solution with the final solution of the best of the processes assessed.

2. Results

For the present study, an Fe-DES system was fabricated with choline chloride and citric acid to which iron was added. This catalyst was used for the Fenton and E-F reactions and PMS (A-PMS and A-E-PMS). The catalyst was characterized by different analytical techniques in order to obtain the maximum information and knowledge about its properties. The techniques performed are listed and explained in Section 3.

2.1. Catalyst Characterisation

The synthesis of the Fe-DES is described in Section 3.2, followed by analysis of the effectiveness of this synthesis. The FTIR analysis (Figure 1a) showed three peaks, at 695, 530 and 447 cm^{-1}, corresponding to the Fe-O bond stress modes of Fe_2O_3-type iron oxide. The bands between 986 and 1200 cm^{-1} may have been due to C-O and C-OH bond tensions. In addition, a band was revealed in the spectrum around 3408 cm^{-1}, which was constituted by the modes of O-H bond tension, with an emergent bending at 1634 cm^{-1}. RAMAN analysis (Figure 1b) confirmed the presence of Fe_2O_3, specifically in the form of hematite, in two modes: in A1g mode at positions 227.3 and 495.8 cm^{-1}, and in Eg mode at positions 248.3, 295.5, 412.9 and 617.6 cm^{-1}. The same peaks corresponding to the two modes of the hematite, A1g and Eg, were found in the study of Talibawo et al. [26]. Here, they obtained hematite nanoparticles through a hydrothermal process. The RAMAN study also revealed a symmetric C-N tension at position 663.3 cm^{-1}, as can be seen in Figure 1b.

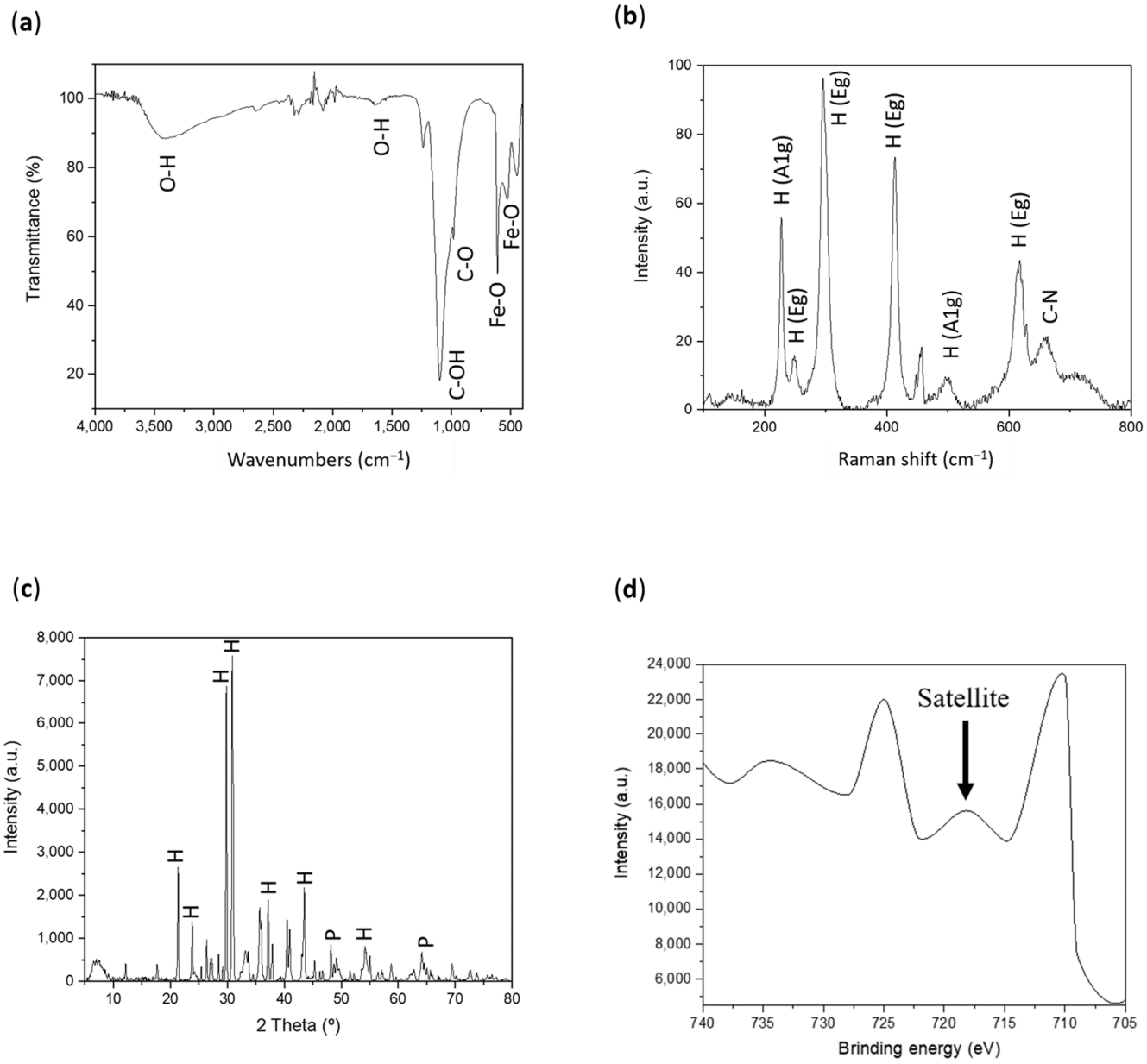

Figure 1. Fe-DES characterisation: (**a**) FTIR; (**b**) RAMAN, where H: hematite; (**c**) XRD, where H: hematite and P: propionamide; (**d**) XPS.

The characterisation was completed using the XRD analytical technique (Figure 1c), which again confirmed the presence of hematite (JPDES 00-024-0072), and indicated the appearance of propionamide (C_3H_7NO, JPDES 00-022-1772) as a possible compound in the catalyst composition. The hematite code has been confirmed and found in other studies [27,28]. Specifically, Khamis et al. [29] suggested that this code corresponded to hematite of rhombohedral crystalline structure. In their work, they manufactured and characterized nanocomposites for microwave-shielding applications. After the process, they obtained hematite; as can be seen in their reported SEM figures, the forms they observed were very similar to those detected in the TEM images obtained in the present study, which are shown in the microscopic characterisation images in Figure 2a–d.

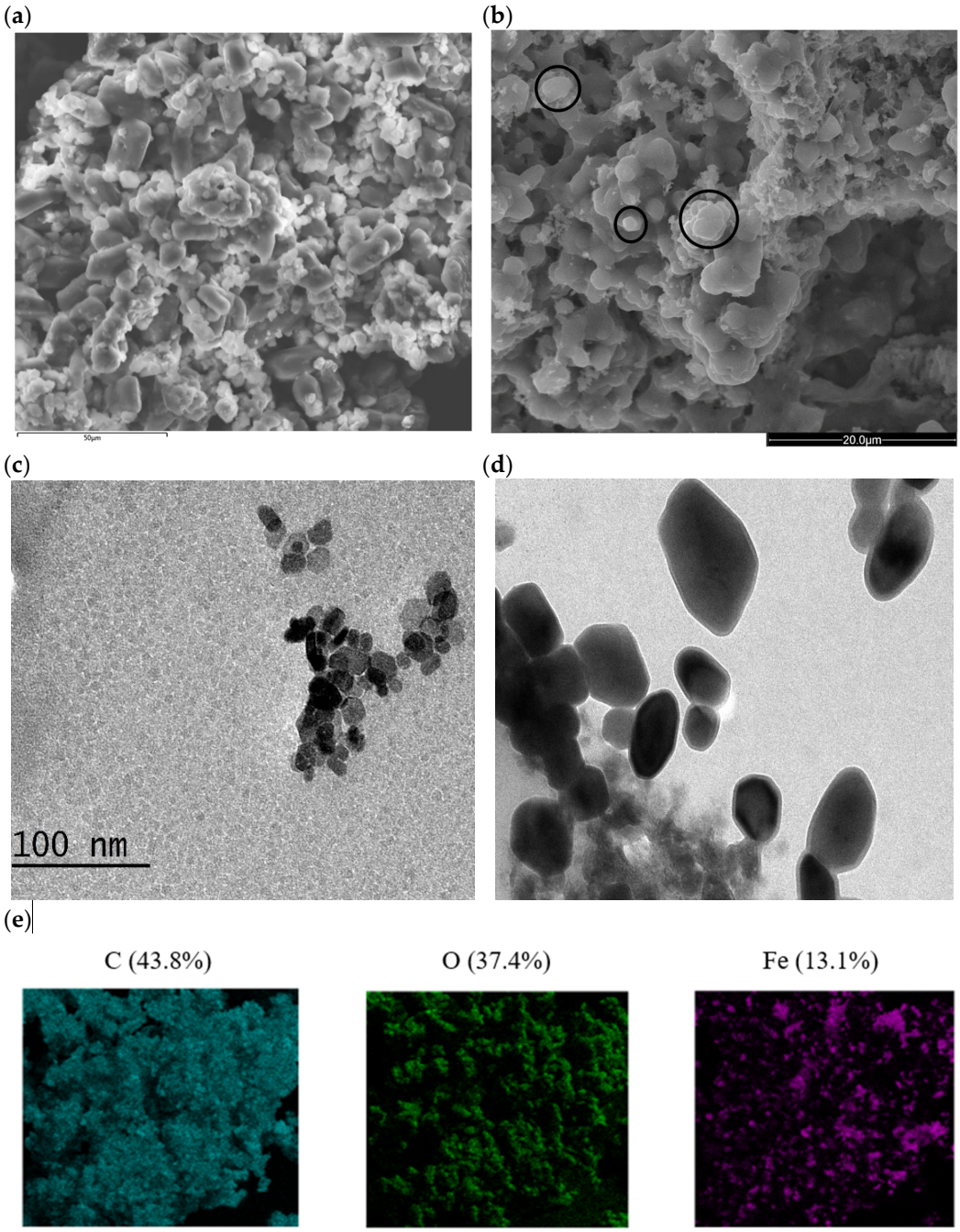

Figure 2. Characterisation of the synthesized catalyst: SEM images at (**a**) 50 µm and (**b**) 20 µm, with identification of hematite (indicated in empty circles); TEM images of (**c**) spheres of hematite and (**d**) non-uniform spheres of hematite; (**e**) mapping of the catalyst, including data of the main components determined by EDS analysis.

Finally, XPS analysis revealed an elemental composition formed mainly by three compounds, which, in order of appearance, were carbon, oxygen and iron. Nitrogen was also identified in the catalyst composition. The XPS analysis helped to provide more specific information on the oxidation state of iron (Figure 1d). The results of the analysis revealed a predominant Fe^{+3} state since the Fe^{+3}-rich species had a characteristic satellite located between 8 and 9 eV at energies higher than the main Fe2p3/2 peak. This peak was typical of iron in the XPS analysis, along with Fe2p1/2. As can be seen in the figure, the first peak (around 710 eV) was narrower and stronger than the second (around 725 eV); the peak area of the first (Fe2p3/2) was greater than that of the second (Fe2p1/2) due to

spin-orbit coupling (j-j) [30]. In this case, the sample had a satellite around 718–719 eV, which corresponded to the Fe^{+3} chemical environment (black arrow, Figure 1d).

Kwon et al. [31] worked on the reversible conversion of mesoporous iron oxide for lithium-ion batteries. In their study, a small satellite was observed through XPS analysis before the cycle, between the Fe2p3/2 and Fe2p1/2 peaks, which disappeared after five cycles of use. An analysis of O 1s was also performed using the XPS technique, which was found to be deconvoluted into two peaks: first, an O 1s oxides peak (529.81 eV), and second, a COO-carboxylic O 1s peak (532.93 eV). In Mohite et al. [32], the analysis of O 1s in a sample containing titanium was deconvoluted into three peaks; the two peaks at 528.5 and 531.5 eV were assigned to oxygen binding with a metal oxide and a hydroxyl backbone, respectively. However, for the third peak (529.9 eV, the same range as the detection of oxides in this work), the authors found evidence that it came from surface defects generated by TiO_2.

Regarding the microscopic analysis, the images taken revealed a homogeneous sample with the main elements well distributed (Figure 2a). In the specific case of iron, which is known to form hematite together with oxygen, non-uniform spheres were observed (Figure 2b), with sizes smaller than 100 nm (Figure 2c), consistent with the observations of other authors [33]. Non-uniform spheres were also observed in the TEM analysis (Figure 2d). Both analyses revealed key information about the material, since the catalytic activity of hematite is directly determined by the catalyst surface, the exposed crystal faces (area), as well as its geometric shape [34,35]. The non-uniform spheres present more exposed crystal faces, which is related to a higher density of iron atoms in the plane, and, in turn, higher activity of the hematite nanocrystals, when iron cations are attached to oxygen [36]. EDS analysis (Figure 2e) was also carried out on the samples, confirming the appearance of the three main elements, which, in descending order, were carbon (43.8%), oxygen (37.4%), and iron (13.1%), as indicated by the XPS analysis. Hematite, as reported in many studies available in scientific databases [37–41], has been shown to perform very well as a catalyst. So, once the manufactured material was analysed, it was used as a catalyst in various AOPs, as detailed in the following points.

2.2. Degradation of SMX: Fenton and PMS

The degradation of the antibiotic SMX, at a concentration of 25 mg/L, was initially carried out through the generation of hydroxyl radicals by the Fenton process. For this, Fe-DES was used in three concentrations: low concentration, medium concentration, and high concentration (0.26, 0.53, and 0.81 mM of iron, respectively. Table 1).

Table 1. Leaching iron values in the Fenton, E-F, A-PMS and A-E-PMS treatments.

Treatment	Catalyst Concentration Level and Leaching (%)		
	Low (0.26 mM)	**Medium (0.53 mM)**	**High (0.81 mM)**
Fenton	50.54	30.89	27.85
E-F	24.93	15.90	13.39
A-PMS	8.19	6.27	6.52
A-PMS (pH 4)	-	-	8.03
A-PMS (pH 3)	-	-	10.32
A-E-PMS	-	-	5.13

Before carrying out the degradation tests, an adsorption assay was performed for the three catalyst concentrations to find out if part of the elimination achieved could be by adsorption. The results were disregarded, since less than 1% adsorption occurred for all catalyst concentrations.

As already mentioned, heterogeneous catalysts are important within the circular economy because they have unique advantages over homogeneous catalysts [42]. Therefore,

in this first degradation assay, the feasibility of a "green" process was assessed in an acidic medium (pH 3), initially testing the catalyst with the lowest concentration (0.26 mM). Based on this, to determine which would be the optimal peroxide concentration in this process, the amount was calculated based on the iron concentration, administering a proportional H_2O_2 concentration, according to the relationship previously established by Sanromán's research group [43,44], where the optimum H_2O_2 concentration was found to be 10 times the iron concentration. Therefore, for the first test (catalyst: 0.26 mM iron), a 2.6 mM concentration of H_2O_2 was used.

As can be seen in Figure 3, the degradation achieved for 6 mM Fe-DES was only 15.63%, which led to testing the other two, reaching levels of 24.22 and 34.53% for 0.53 and 0.81 mM of iron, respectively, all in a test time of 120 min. To continue with the purpose of achieving a process as ecological as possible, no modification on the concentration of hydrogen peroxide (2.6 mM H_2O_2) was carried out when the concentration of the catalyst was increased.

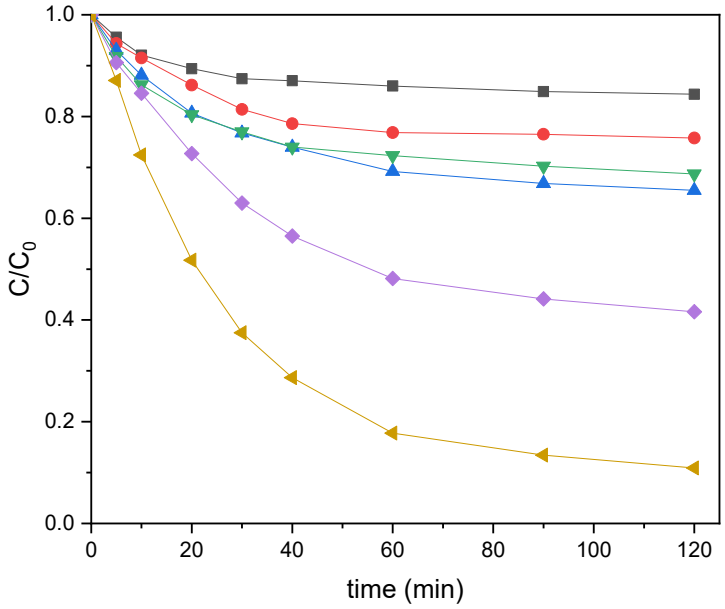

Figure 3. Degradation profiles with Fe-DES: 0.26 mM (black line), 0.53 mM (red line) and 0.81 mM (blue line) concentrations for the Fenton treatment; and 0.26 mM (green line), 0.53 mM (purple line) and 0.81 mM (yellow line) concentration for the A-PMS treatment.

The behaviour of the three reactions was similar, with the rate of elimination slowing down at 40 min for the 0.26 mM catalyst, and at 60 min for the 0.53 and 0.81 mM catalysts. Due to the lack of effectiveness observed for this process, and as already mentioned, it was decided not to increase the H_2O_2 concentration according to the mentioned relationship (10× the iron concentration), without first studying leaching.

Table 1 shows the leaching values for the three catalysts, which, in increasing order of concentration, were 50.54, 30.89 and 27.85% with respect to the initial iron concentration. Based on these results, the system was inferred to be operating in a hybrid mode of homogeneous and heterogeneous catalysis. At this point, the possibility of carrying out tests with a sufficient proportion of hydrogen peroxide was ruled out due to the high leaching detected. In addition, values of 5.3 and 8.1 mM of H_2O_2 would needed to have been added, which would not have been very ecologically friendly, and could have resulted in an excess of hydrogen peroxide in the medium, which would not have favoured the process, but quite the opposite, as expressed by Equation (8).

$$Fe^{2+} + HO^{\bullet} \rightarrow Fe^{3+} + OH^{-} \quad (8)$$

$$H_2O_2 + HO^{\bullet} \rightarrow H_2O + HO_2^{\bullet} \quad (9)$$

The low catalytic activity of the process is noteworthy, taking into account the large amount of iron leached into the medium, as it converted, as previously stated, into a hybrid process (homogeneous and heterogeneous). This low activity can be explained by the high level of leaching into the medium, which varied from 7.5 mg/L to 12.5 mg/L, for low to high catalyst concentration, respectively. As other authors have reported, a high level of catalyst leaching may be unfavourable when the generation of hydroxyl radicals is insufficient. Furthermore, a large amount of ferrous ions in the medium could react with hydroxyl radicals, reducing the active sites for oxidation [45,46] and the electron transfer reaction [47] (Equation (9)).

To address these drawbacks, PMS, which has often been used as an oxidant for the removal of micropollutants [48], was tested as a possible solution to the high leaching resulting from the Fenton treatment. For this, a low concentration of PMS was used, equal to the concentration of hydrogen peroxide (2.6 mM), and the catalyst was used as a PMS activator (A-PMS).

Following the approach described in the previous section, A-PMS was tested in three catalyst concentrations. The obtained results were much better than for the process using hydroxyl radicals, as shown in Figure 3. In 120 min, for 0.26 mM Fe-DES, the elimination levels reached 31.31%, for 0.53 mM, 58.37%, and for 0.81 mM, 89.19%.

All tests were carried out at natural pH (4.91 for the low catalyst; 5.13 for the medium catalyst; 5.45 for the high catalyst). The pH variation was recorded throughout the process, decreasing to around 0.7, 0.8 and 0.9 points, respectively (final pH 4.26, 4.36 and 4.58 for low, medium, and high catalysts).

For more in-depth study, degradation kinetics were used, where the degradation behaviour of SMX could be determined using a pseudo-first-order reaction kinetics model (Equation (10)). As expected, the speed was faster than in Fenton (Table 2). Specifically, the rate constant (k) was 1.5 times higher in the low catalyst (0.26 mM), 2 times higher in the medium catalyst (0.53 mM), and 3 times higher in the high catalyst (0.81 mM), compared to Fenton, with kinetic constant values of 0.0071, 0.0143, and 0.0319 (1/min), respectively.

$$\frac{dC}{dt} = -kC \quad (10)$$

where: C (mg/L) is the pollutant concentration, t (min) is the time, and k (1/min) is the pseudo-first-order reaction kinetic coefficient.

Table 2. Kinetic data obtained in the Fenton, A-PMS (at different pHs), E-F and A-E-PMS treatments.

Treatment	Catalyst Concentration Level (mM)					
	0.26	**0.53**	**0.81**	**0.26**	**0.53**	**0.81**
	k (1/min)			**R^2**		
Fenton	0.0042	0.0066	0.0087	0.9559	0.9895	0.9781
A-PMS	0.0071	0.0143	0.0319	0.9713	0.9948	0.9982
A-PMS (pH 4)	-	-	0.0330	-	-	0.9985
A-PMS (pH 3)	-	-	0.0379	-	-	0.9991
E-F	0.0044	0.0079	0.0091	0.9946	0.9909	0.9910
A-E-PMS	-	-	0.0420	-	-	0.9938

With reference to Table 1, leaching was again investigated. The leaching values dropped dramatically to 8.19, 6.27 and 6.52% (0.26, 0.53, and 0.81 mM, respectively). In

this case, leaching could have been reduced for various reasons. One reason may have been increase in the pH of the solution, since it is known that greater leaching occurs in acid media in processes involving AOPs [49,50]. On the other hand, as seen in the characterisation section, the Fe-DES still contained nitrogen in small proportions (found in all analyses except FTIR). Several authors have reported the activation of PMS by nitrogen [51–53]. Wang et al. [54] activated PMS with nitrogen-doped graphene for the elimination of the same antibiotic as in this work, SMX, obtaining 92% elimination in 240 min. The activation carried out at PMS could cause less leaching due to activation and consequent increase in the speed of action of PMS and the Fe^{2+} regeneration on the surface, causing fewer losses. The synergistic effects of applying iron nanocomposites and nitrogen heteroatoms can also result in confinement between layers that minimizes leaching problems, and, therefore, secondary iron contamination [55–57].

The next step was to try to improve this process by acidifying the assay. It has been emphasized since the beginning of this work that the objective was to maintain a low-cost treatment profile, so PMS treatment by simple iron activation (A-PMS) was appropriate. It must be taken into account that application of A-PMS with the 0.81 mM catalyst achieved an elimination of 89%, which translated into 22.84 mg/L of SMX eliminated in 120 min. However, the attempt to further improve this percentage consisted in acidifying the test at two points, at pH 4 and pH 3 (natural pH around 5). As the best test performance with A-PMS was with the high catalyst, with reduced leaching, only the acidification test was performed for the high catalyst (0.81 mM).

The results are shown in Table 2 in the form of kinetic data assessing the reaction rates of the acidifications. The kinetic constant increased slightly as the conditions became more acidic (from pH 5, natural, to pH 3) to 0.0319, 0.0330 and 0.0379 (1/min), respectively. When pH was modified to 4, the elimination value increased by 1% with respect to the test at natural pH (from 89.10 to 90.44%). The pH varied from 4 (initial, time 0 min) to 3.44 (final, time 120 min). Regarding the modified pH of 3, the increase in elimination was a little more notable, degrading almost 95% of the initial 25 ppm of SMX. The pH varied throughout the test, decreasing from 3 to 2.36. Therefore, the PMS modified at pH 3 managed to remove 24.29 ppm, which was different from the PMS at natural pH (1.45 ppm extra removed). Acidifying the medium did not seem justified to increase elimination by approximately 5% (1.45 ppm).

In other published works where different pHs have been tested in the treatment with PMS, no great differences in elimination have been observed [58,59]. For example, in the case of the elimination of carbamazepine by means of PMS carried out by Fan et al. [60], the best result was achieved when working at the natural pH of the solution (around 6.3).

To continue the same scheme, and if relevant, iron leaching was also investigated in the PMS tests with artificially changed pH. The achieved leaching values exceeded that of the test at natural pH. As the process became more acidic, leaching was greater (Table 1). It should be recalled that the leaching for PMS at natural pH was 6.52 and for PMS at modified pHs increased to 8.03% (at pH 4) and 10.32% (at pH 3). Thus, operating at a more acidic pH only a 5% of increase in the degradation was achieved, but with more leaching at these acidic pH values, and the best result remained that for PMS at natural pH.

2.3. Electro-Degradation of SMX: Electro-Fenton (E-F) and Electro-Activated PMS (A-E-PMS)

The degradation of the SMX was carried out in a second stage, through the electro-generation of hydroxyl radicals, through the E-F process. For this, the same concentrations of Fe-DES were tested in an electrochemical cell formed by two electrodes of conductive PLA at a pH similar to those used in the Fenton treatment (pH = 3).

As can be seen in Figure 4, the three tests underwent a progressive elimination of the pollutant as the hydrolysis time increased. To a lesser extent, for 0.26 mM Fe-DES, a lack of activity was evidenced from minute 90, reaching a total elimination of 23.27%. For 0.53 mM Fe-DES, the elimination was 37.09%, while, for 0.81 mM Fe-DES, the result obtained was 48.25% of degraded SMX.

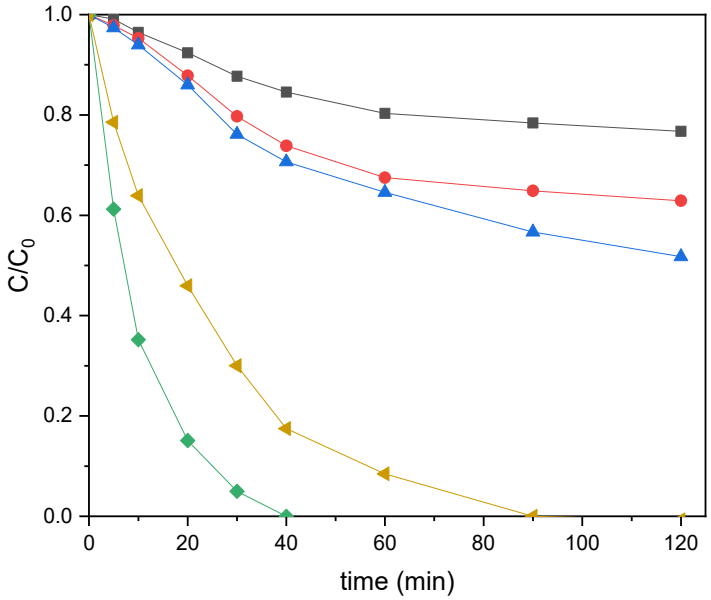

Figure 4. Degradation profiles with 0.26 mM (black line), 0.53 mM (red line) and 0.81 mM (blue line) Fe-DES concentrations for the Fenton treatment, and with 0.81 mMFe-DES concentration (yellow line) for the A-E-PMS treatment, which was also tested in homogeneous mode (0.81 mM, green line).

Regarding the degradation kinetics (Table 2), the rate constants (k) in increasing order of catalyst concentration were 0.0044, 0.0079 and 0.0091 (1/min), respectively; the values were very similar to those obtained in the Fenton process. This indicates greater activity on the part of the more concentrated catalyst, despite the fact that in two hours of treatment it did not reach 50% of the pollutant degraded. The option of extending the treatment in time to obtain better elimination did not seem to be a viable one, since the reaction slowed down in the final minutes, and the increase in time would have led to an increase in energy consumption that would probably not have been compensated, taking into account the best results from A-PMS.

An iron leaching study was carried out to evaluate the functionality of the studied catalyst when applying an electric field. The data, shown in Table 1, revealed that the catalyst led to leaching in different proportions: 24.93% leaching in the lowest concentration (0.26 mM), 15.90% in the medium concentration (0.53 mM) and 13.39% in the highest concentration (0.81 mM).

One of the many advantages offered by E-F is the in situ electro-generation of Fe^{2+} (Equation (11)), which can reduce iron leaching [61,62]. This explains the lower leaching rate obtained in the electric field test. In addition, taking into account that the application of an electric field increased the temperature of the electrochemical reactor during the test, Panizza et al. [63] stated, in their study of the removal of dyes using E-F, that an increase of 10 °C in temperature (from 25 to 35 °C) may be associated with an increase in the rate of reaction with hydroxyl radicals. In this way, in their work, they obtained great efficiencies in COD reduction by increasing the temperature by 10 °C, with the higher speed of the process decreasing leaching.

$$Fe^{3+} + e^{-} \rightarrow Fe^{2+} \quad (11)$$

Despite the better elimination and reduction of leaching compared to the Fenton treatment, A-PMS continued to provide the best results. In order to improve this process, one last test was performed: the combination of electric current with PMS activated by iron from the heterogeneous catalyst. To do this, the new assay merged activation and electrical current (A-E-PMS). Based on the results achieved in the previous use of A-PMS, the test was carried out at natural pH. The current applied in the A-E-PMS was the same as for the E-F process (20 mA). This test was performed with the same PLA electrodes made in the laboratory. The iron catalyst concentration was considered optimal (0.81 mM).

As can be seen in Figure 4, the degradation profile of SMX with A-E-PMS was much faster, achieving complete elimination of the contaminant under study (25 ppm). In addition, the elimination was achieved after 90 min of testing, 30 min less than the time set in all the tests carried out before. Therefore, the difference with A-PMS (approx. 90% elimination in 120 min) was very obvious, obtaining total elimination in a shorter test time, with consequent saving of time and energy.

In order to guarantee success of the synthesis carried out on the basis of DES to obtain an Fe-DES heterogeneous catalyst, a comparison with iron in homogeneous mode was performed. For this, iron sulfate, very commonly used in this type of process, was used with the same concentration of iron as the catalyst that worked best (0.81 mM). The test was carried out under the same conditions as for the A-E-PMS. As can be seen in Figure 4, the A-E-PMS achieved 100% removal in 40 min. Despite achieving total elimination in a shorter period than the heterogeneous process, the drawbacks of the homogeneous catalyst and the advantages offered by the heterogeneous catalyst allows to state that Fe-DES remains a good catalyst candidate.

As in the previous studies, the percentage of leaching was evaluated as an essential part of the validation of the process. In this case, the A-E-PMS resulted in less leaching than the A-PMS, reaching a value of 5.12%. As with the Fenton process, when applying electric current, a significant reduction in leaching was obtained; in the case of PMS, the pattern was the same. Therefore, the A-E-PMS had a further advantage for the rapid degradation, which was obtaining the minimum iron leaching of all the tests proposed in this work. Regarding the kinetic constant, A-E-PMS resulted in the highest process speed (k = 0.0420 (1/min), Table 2). In terms of energy consumption (EC, Equation (12)), comparing A-E-PMS with the E-F treatment, the difference was notable. For the former, in an elimination time of 90 min (100% of SMX eliminated), the consumption was 0.71 kWh, with an average voltage of 23.8 V. For the E-F, the consumption was 0.98 kWh for a 120 min removal time (approx. 50% of SMX removed), with a mean voltage of 24.5 V.

$$EC\ (\text{kwh}) = I \times V \times \frac{t}{60} \tag{12}$$

where: I is the intensity (A), V is the average of the consumed voltage and t is the time of assay (min).

The improvement in degradation could be a consequence of the appearance of two major oxidants, the sulfate radical and the hydroxyl radical (Equation (7)). In some studies, the PMS was activated with electrical current [64–66]. In others, as has already been commented, the activation was performed using a metal [67,68]. However, several studies have combined the two techniques to improve the removal efficiency of organic contaminants [69–72], with joint application proving to be very successful. Therefore, this work brings together several novelties that could open new lines of research, both in the effective use of Fe-DES and in A-E-PMS treatment, combining two of the most oxidising radicals, hydroxyl and sulfate.

2.4. Mineralisation Study

In order to know how the process evolved during the degradation of SMX by A-E-PMS, the degradation intermediates were studied. Figure 5 shows the carboxylic acids detected throughout the test time (120 min). Even though the A-E-PMS assay reached 100% elimination in 90 min, for the degradation intermediates, the time taken was 120 min. This reasoning is based on interest in seeing how the carboxylic acids evolved throughout the A-E-PMS process while the contaminant still existed (first 90 min), but also in how it evolved once the initial contaminant (SMX) had been transformed into other compounds (from 90 to 120 min).

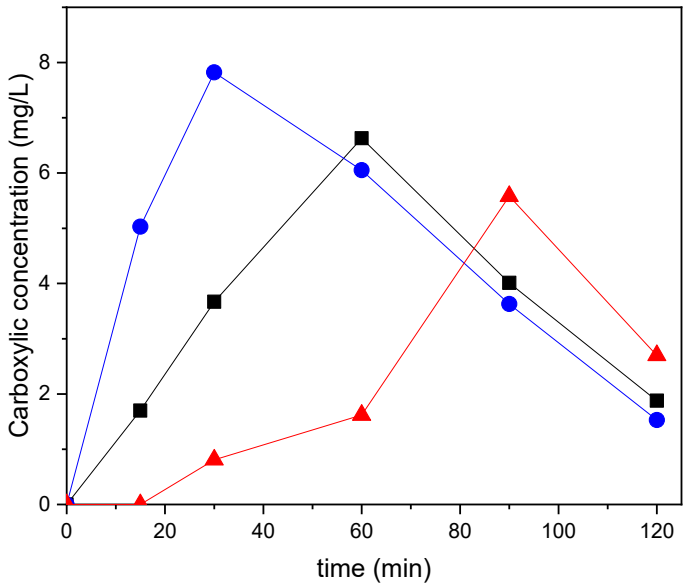

Figure 5. Carboxylic acids detected in the A-E-PMS treatment with high catalyst, where the blue line represents succinic acid, the black line corresponds to oxalic acid, and the red line, acetic acid.

Fundamentally, three carboxylic acids were detected: oxalic, succinic, and acetic acid. These short chain acids reached their maximum concentration in treatment times of 30 min (succinic acid), 60 min (oxalic acid) and 90 min (acetic acid). The trend in these organic acids, as seen in Figure 5, decreased as the test progressed, and, at the end time (120 min), the three acids detected were close to zero. These carboxylic acids have been detected by other authors in the degradation of SMX via PMS [73,74]. In addition, they have also been detected in the degradation of this antibiotic by E-F treatment [75,76]. In this work, since PMS was activated with iron, it may be possible that the degradation route followed by SMX was in some respects comparable to that of E-F. Of the three, the longest chain acid is succinic, which was the first to appear, along with oxalic. The succinic acid reached a high concentration more quickly, which decreased over time. The oxalic acid, also from the beginning, showed a more progressive increase and slow elimination.

As already mentioned in a previous study [14], oxalic acid generally forms intermediate complexes with iron that are sometimes more stable than the original compounds themselves, and make the degradation of carboxylic acids slower. In this case, the elimination of the oxalic acid is similar to that of the succinic acid, and, since the iron is deposited on a heterogeneous catalyst, it seems that it helps to avoid this problem. Finally, acetic acid, the shortest chain, prior to mineralisation appeared after just 15 min of the degradation test.

2.5. Toxicity Test

Using the same test by which the degradation intermediates were studied (A-E-PMS at natural pH), a simple ecotoxicity study was carried out. The sensitivity of this test depends on the selected bioindicator [77]. For this study, lentil seeds were selected, representing the bioindicator, and tap water, representing the control. The selected samples corresponded to the initial solution of SMX (25 ppm) and a final sample of the A-E-PMS treatment after 120 min. Both samples shared the same pH since the final sample of A-E-PMS and the initial solution of 25 ppm of SMX were close to 4.5.

As can be seen in Table 3, the germination ratio (GR) was 100% with the control and with the final solution of A-E-PMS. However, for the initial solution (25 ppm SMX), the germination rate decreased to 80%. When the germination rate was observed, large differences were seen, both in the initial growth rate (48 h) and the final rate (72 h), between the solutions used to irrigate the seeds. The germination index (GI) at 72 h, varied between the control, the initial solution, and the final A-E-PMS test (GI = 1, 0.23 and 0.83, respectively). The germination with the final test solution was three times higher than the index with

the initial SMX solution. In addition, with this solution, a decrease in the index could be observed between 48 and 72 h. This appears to be a delay in the growth rate, indicating toxicity of the initial sample not observed in the final sample, which had no impact on the growth of the seeds and again validated the effectiveness of the proposed process.

Table 3. Toxicity test data for control, initial (25 mg/L SMX) and final after treatment (A-E-PMS) samples.

Sample	Time (h)	GR (%)	RL	TL	GI (%)
Control	48	100	0.44 ± 0.09	1.58 ± 0.49	100
	72	100	1.22 ± 0.16	3.46 ± 0.72	100
25 mg/L SMX	48	80	0.20 ± 0	0.50 ± 0.07	36
	72	80	0.35 ± 0.19	1.15 ± 0.32	23
A-E-PMS	48	100	0.20 ± 0	0.86 ± 0.33	45
	72	100	1.02 v 0.53	2.66 ± 0.44	83

3. Materials and Methods

3.1. Reagents

Sulfamethoxazole, which was supplied by Sigma-Aldrich (Saint-Louis, MI, USA), was evaluated as a pollutant; its characteristics are described in Puga et al. [76]. For the catalyst synthesis, choline chloride, citric acid, $FeCl_2.4H_2O$ and $FeCl_3.6H_2O$ were obtained from Sigma-Aldrich and KOH from VWR International (Radnor, USA). For the assays, H_2O_2, Oxone® and Na_2SO_4 were provided by Sigma-Aldrich and H_2SO_4 was furnished by Fischer Chemical (Waltham, USA). The conductive PLA filament used in the 3D printed electrodes was obtained from 3DCPI. The organic solvents were HPLC grade from Fischer Scientific (Hampton, USA) and Sigma-Aldrich. For all assays, Milli-Q grade water was used as a solvent for the preparation of the solutions.

3.2. Catalyst Synthesis

The catalyst was manufactured based on the study performed by Sakthi et al. [78]. Deep eutectic solvent was prepared by mixing (600 rpm) and heating (80 °C) choline chloride (139.62 g/mol) and citric acid (192.12 g/mol) in a molar ratio for 2 h. For the synthesis of iron oxide nanoparticles, 3.9813 g of $FeCl_2.4H_2O$ (20 mM) and 8.1091 g of $FeCl_3.6H_2O$ (30 mM) in the molar ratio 1:1.5, respectively, were added to the above DES for 20 min. Finally, 40 g (712.94 mM) KOH was added and stirred for 1 h. The nanoparticles were washed several times with ethanol and distilled water and dried in a hot air oven.

3.3. Catalyst Characterisation

3.3.1. Fourier Transform Infrared Spectroscopy (FTIR)

Samples, previously dried overnight (60 °C), were compressed in a KBr pill and analysed between 400 and 4000 cm^{-1} in a Nicolet 6700 FTIR spectrometer (ThermoFisher Scientific, Waltham, MA, USA) (C.A.C.T.I., Universidade de Vigo).

3.3.2. Raman Spectroscopy

Raman spectroscopy was carried out using a Horiba Jobin Yvon HR800UV spectrometer with Ar diode and HeNe ultraviolet lasers (Horiba Ltd., Kyoto, Japan). The detector used, suitable for UV, visible and infrared, was an air-cooled CCD (1024 × 1056 pixels of 26 microns) (C.A.C.T.I., Universidade de Vigo).

3.3.3. X-ray Diffraction (XRD)

XRD was performed using a Siemens D5000 X-ray powder diffractometer (Siemens Ag, Munich, Germany) through drying and grinding of the samples to less than 20 µm (T = 4 to 80 °C) (C.A.C.T.I., Universidade de Vigo).

3.3.4. XPS

XPS analysis of the samples was performed using a Thermo Scientific NEXSA (XPS) instrument equipped with aluminium Kα monochromatized radiation at 1486.6 eV X-ray source (ThermoFisher Scientific, Waltham, U.S.). Neutralisation of the surface charge was performed using both a low-energy flood gun (electrons in the range 0 to 14 eV) and a low-energy argon ions gun (C.A.C.T.I., Universidade de Vigo).

3.3.5. Microscopy Characterisation

Microscopy characterisation was carried out by scanning electron microscopy (SEM) carried out on a JEOL JSM-6700F-EDS Oxford Inca Energy 300-20 kV microscope (Oxford Instruments, Abingdon, UK), combined with energy dispersive spectroscopy (EDS) for chemical microanalysis. In addition, transmission electron microscopy (TEM) was performed with a JEOL JEM-1010 high-contrast transmission electron microscope 100 kV (Oxford Instruments, Abingdon, U.K.) (C.A.C.T.I., Universidade de Vigo).

3.4. Experimental Methods

3.4.1. Adsorption Studies

Adsorption experiments were performed in 50 mL Erlenmeyer flasks containing 0.26, 0.53, and 0.81 mM of iron in 40 mL of 25 mg/L SMX solution. The suspension was stirred in an incubator Thermo Scientific MaxQ800 (ThermoFisher Scientific, Waltham, MA, USA) at 150 rpm and 25 °C for 120 min. All experiments were duplicated and liquid aliquots (1 mL) were taken throughout the experiment to measure analyte concentration. All samples were centrifuged at 10,000 rpm for 5 min, and the supernatant was separated to analyse the removal percentage.

3.4.2. Degradation Studies

Fenton/A-PMS were developed in a 50 mL capacity cylindrical reactor with 40 mL of the SMX solution containing 0.26, 0.53, and 0.81 mM of iron catalyst. Hydrogen peroxide/Peroxone® was added initially at a concentration of 0.26 mM. The solution (pH = 3) was kept stirring at 150 rpm IKA RCT Basic (IKA®-Werke GmbH & Co., Staufen, Germany) and 25 °C for 120 min. All experiments were duplicated and liquid aliquots (1 mL) were taken throughout the experiment to measure analyte concentration. All samples were centrifuged at 10,000 rpm for 5 min, and the supernatant was separated to analyse the removal percentage.

3.4.3. Electro-Degradation Studies

E-F/A-E-PMS were developed in a 50 mL capacity cylindrical reactor with 40 mL of the SMX solution containing 0.26, 0.53, and 0.81 mM of catalyst. In the case of A-E-PMS, Peroxone® was added initially at a concentration of 0.26 mM. The solution (pH = 3) was kept stirring at 150 rpm (IKA RCT Basic) and 25 °C for 120 min. Electrical current (20 mA) was applied through a power supply Siglent SPD3303C (Siglent Technologies, Shenzhen, China). All experiments were duplicated and liquid aliquots (1 mL) were taken throughout the experiment to measure analyte concentration. All samples were centrifuged at 10,000 rpm for 5 min, and the supernatant was separated to analyse the removal percentage.

3.5. Analytical Procedures

3.5.1. Determination of SMX

SMX (λ = 274 nm) removal was measured by HPLC (Agilent 1100) using an ion-exclusion Zorbax Eclipse XDB (8%) column (150 $\times$ 4.6 mm; Agilent, Santa Clara, CA, USA). The column was maintained at room temperature and the mobile phase, consisting of acetonitrile and 1.5% acetic acid (10:90 v/v) solution, was pumped for 20 min (gradient mode: 1 L/min).

3.5.2. Determination of Carboxylic Acids

Generated short-chain carboxylic acids were determined by HPLC (Agilent 1100) using ion-exclusion RezexTM ROA-Organic Acid H+ (300 × 7.8 mm; Phenomenex, Torrance, CA, USA). The column was maintained at 55 °C and the mobile phase, consisting of a 0.025 M H_2SO_4 solution, was pumped for 30 min (isocratic mode: 0.5 L/min).

3.5.3. Iron Concentration

The initial iron content of the catalyst, as well as the iron leaching value in the different tests, were measured by the 1,10-phenantroline spectrophotometric method (Standard methods) (Jasco V-630). Solid samples were previously digested (Danish Standard method DS259).

3.5.4. Toxicity Test

The toxicity was evaluated through the germination rates of the samples using lentil seeds as reported in a recent paper [14]. The tests were carried out on five lentils placed on filter paper in glass Petri dishes (120 mm) grown in the dark at 25 °C for 72 h. The solutions used were the control (tap water), initial SMX solution, and the final treated solution. The parameters measured included root length (*RL*), root and hypocotyl length (TL), and germination ratio (*GR*; Equation (13)) and germination index (*GI*; Equation (14)) [77].

$$GR\ (\%) = \frac{GSS}{GSC} \times 100 \tag{13}$$

$$GI\ (\%) = \frac{RLS \times GSS}{RLC \times GSC} \times 100 \tag{14}$$

where *GSS* is the germinated seeds in the sample, *GSC* is the germinated seeds in the control, *RLS* is the root length of the sample, and *RLC* is the root length of the control.

4. Conclusions

In this work, two alternatives for the degradation of the antibiotic SMX were proposed: one by use of hydroxyl radicals, with two processes: Fenton and E-F, and another by use of radical sulfate, with PMS activated with iron (A-PMS). Finally, an activated degradation with iron and with the application of an electric field (A-E-PMS) was carried out, obtaining hydroxyl and sulfate radicals in the same test. For these degradation proposals, a new catalyst synthesized on deep eutectic solvents was developed, composed of choline chloride and citric acid, to which iron was added. This heterogeneous catalyst acted as a reagent in the Fenton and E-F process and as a process activator by PMS, and was characterized by microscopy (SEM-EDS and TEM) and FTIR, RAMAN, XRD and XPS structural analysis. The characterisation revealed that the iron was in the form of hematite; the stability of the catalyst was obtained by means of the minimum variation obtained in all the tests, which were carried out in duplicate. Furthermore, as a novel alternative to electrochemical testing, two inexpensive PLA electrodes were successfully tested. The best result was obtained with the combination of A-E-PMS, reaching complete elimination (25 mg/L of SMX) in 90 min, without the need to modify the pH, and with leaching values of 5%. In the study of degradation intermediates, three short-chain carboxylic acids (oxalic, succinic and acetic) were detected, which, together with the toxicity test, demonstrated the feasibility of Fe-DES to degrade priority pharmaceutical compounds for study, such as in the case of SMX. In addition, it was shown that the novel combination of hydroxyl radicals and sulfate can be very beneficial in these fields of research.

Author Contributions: Conceptualisation, A.P. and E.R.; methodology, E.R. and M.A.S.; software, A.P. and E.R.; validation, E.R., M.P. and M.A.S.; formal analysis, A.P.; investigation, A.P.; resources, M.P. and M.A.S.; writing—original draft preparation, A.P.; writing—review and editing, A.P., E.R., M.P. and M.A.S.; visualization, A.P.; supervision, E.R., M.P. and M.A.S.; project administration, M.P. and M.A.S.; funding acquisition, M.P. and M.A.S. All authors have read and agreed to the published version of the manuscript.

Funding: This research was funded through the join 2019–2020 Biodiversa & Water JPI joint call for research proposals, under the BiodivRestore ERA-Net COFUND programme with the Project PCI2022-132941 funded by MCIN/AEI/10.13039/501100011033 and Project PDC2021-121394-I00 funded by MCIN/AEI/10.13039/501100011033, both by European Union Next Generation EU/PRTR and Xunta de Galicia and ERDF (ED431C 2021-43).

Data Availability Statement: Not applicable.

Conflicts of Interest: The authors declare no conflict of interest.

References

1. Ma, D.; Yi, H.; Lai, C.; Liu, X.; Huo, X.; An, Z.; Li, L.; Fu, Y.; Li, B.; Zhang, M.; et al. Critical Review of Advanced Oxidation Processes in Organic Wastewater Treatment. *Chemosphere* **2021**, *275*, 130104. [CrossRef] [PubMed]
2. Ganiyu, S.O.; Martínez-Huitle, C.A.; Oturan, M.A. Electrochemical Advanced Oxidation Processes for Wastewater Treatment: Advances in Formation and Detection of Reactive Species and Mechanisms. *Curr. Opin. Electrochem.* **2021**, *27*, 100678. [CrossRef]
3. Puga, A.; Meijide, J.; Pazos, M.; Rosales, E.; Sanromán, M.A. Electric Field as a Useful Tool to Improve the Poor Adsorption Affinity of Pollutants on Carbonaceous Aerogel Pellets. *J. Mol. Liq.* **2022**, *366*, 120269. [CrossRef]
4. Yuan, Q.; Qu, S.; Li, R.; Huo, Z.Y.; Gao, Y.; Luo, Y. Degradation of Antibiotics by Electrochemical Advanced Oxidation Processes (EAOPs): Performance, Mechanisms, and Perspectives. *Sci. Total Environ.* **2023**, *856*, 159092. [CrossRef]
5. Li, S.; Wu, Y.; Zheng, H.; Li, H.; Zheng, Y.; Nan, J.; Ma, J.; Nagarajan, D.; Chang, J.-S. Antibiotics Degradation by Advanced Oxidation Process (AOPs): Recent Advances in Ecotoxicity and Antibiotic-Resistance Genes Induction of Degradation Products. *Chemosphere* **2023**, *311*, 136977. [CrossRef] [PubMed]
6. Santos, M.C.; Antonin, V.S.; Souza, F.M.; Aveiro, L.R.; Pinheiro, V.S.; Gentil, T.C.; Lima, T.S.; Moura, J.P.C.; Silva, C.R.; Lucchetti, L.E.B. Decontamination of Wastewater Containing Contaminants of Emerging Concern by Electrooxidation and Fenton-Based Processes—A Review on the Relevance of Materials and Methods. *Chemosphere* **2022**, *307*, 135763. [CrossRef]
7. Moradi, M.; Vasseghian, Y.; Khataee, A.; Kobya, M.; Arabzade, H.; Dragoi, E.N. Service Life and Stability of Electrodes Applied in Electrochemical Advanced Oxidation Processes: A Comprehensive Review. *J. Ind. Eng. Chem.* **2020**, *87*, 18–39. [CrossRef]
8. Santos, G.D.O.; Eguiluz, K.I.B.; Salazar-Banda, G.R.; Saez, C.; Rodrigo, M.A. Testing the Role of Electrode Materials on the Electro-Fenton and Photoelectro-Fenton Degradation of Clopyralid. *J. Electroanal. Chem.* **2020**, *871*, 114291. [CrossRef]
9. Tian, L.; Zhu, M.; Zhang, L.S.; Zhou, L.J.; Fan, J.P.; Wu, D.S.; Zou, J.P. New Insights on the Role of NaCl Electrolyte for Degradation of Organic Pollutants in the System of Electrocatalysis Coupled with Advanced Oxidation Processes. *J. Environ. Chem. Eng.* **2022**, *10*, 107414. [CrossRef]
10. Amor, C.; Fernandes, J.R.; Lucas, M.S.; Peres, J.A. Hydroxyl and Sulfate Radical Advanced Oxidation Processes: Application to an Agro-Industrial Wastewater. *Environ. Technol. Innov.* **2021**, *21*, 101183. [CrossRef]
11. Chen, L.; Ding, D.; Liu, C.; Cai, H.; Qu, Y.; Yang, S.; Gao, Y.; Cai, T. Degradation of Norfloxacin by CoFe2O4-GO Composite Coupled with Peroxymonosulfate: A Comparative Study and Mechanistic Consideration. *Chem. Eng. J.* **2018**, *334*, 273–284. [CrossRef]
12. Meijide, J.; Dunlop, P.S.M.; Pazos, M.; Sanromán, M.A. Heterogeneous Electro-Fenton as "Green" Technology for Pharmaceutical Removal: A Review. *Catalysts* **2021**, *11*, 85. [CrossRef]
13. Shi, J.; Zhang, B.; Wang, W.; Zhang, W.; Du, P.; Liu, W.; Xing, X.; Ding, D.; Lv, G.; Lv, Q.; et al. In Situ Produced Hydrogen Peroxide by Biosynthesized Palladium Nanoparticles and Natural Clay Mineral for Highly-Efficient Carbamazepine Degradation. *Chem. Eng. J.* **2021**, *426*, 131567. [CrossRef]
14. Puga, A.; Rosales, E.; Pazos, M.; Sanromán, M.A. Prompt Removal of Antibiotic by Adsorption/Electro-Fenton Degradation Using an Iron-Doped Perlite as Heterogeneous Catalyst. *Process Saf. Environ. Prot.* **2020**, *144*, 100–110. [CrossRef]
15. Puga, A.; Moreira, M.M.; Figueiredo, S.A.; Delerue-Matos, C.; Pazos, M.; Rosales, E.; Sanromán, M.Á. Electro-Fenton Degradation of a Ternary Pharmaceutical Mixture and Its Application in the Regeneration of Spent Biochar. *J. Electroanal. Chem.* **2021**, *886*, 115135. [CrossRef]
16. Shi, Q.; Deng, S.; Zheng, Y.; Du, Y.; Li, L.; Yang, S.; Zhang, G.; Du, L.; Wang, G.; Cheng, M.; et al. The Application of Transition Metal-Modified Biochar in Sulfate Radical Based Advanced Oxidation Processes. *Environ. Res.* **2022**, *212*, 113340. [CrossRef]
17. Wu, J.; Liang, Q.; Yu, X.; Qiu-Feng, L.; Ma, L.; Qin, X.; Chen, G.; Li, B. Deep Eutectic Solvents for Boosting Electrochemical Energy Storage and Conversion: A Review and Perspective. *Adv. Funct. Mater.* **2021**, *31*, 2011102. [CrossRef]
18. Yu, D.; Xue, Z.; Mu, T. Deep Eutectic Solvents as a Green Toolbox for Synthesis. *Cell Rep. Phys. Sci.* **2022**, *3*, 100809. [CrossRef]

19. Abranches, D.O.; Coutinho, J.A.P. Type V Deep Eutectic Solvents: Design and Applications. *Curr. Opin. Green Sustain. Chem.* **2022**, *35*, 100612. [CrossRef]
20. Hejazikhah, M.; Jamshidi, P. ILSnCl2-MGO Nanocomposite for Efficient Preconcentration of Red 2G via Ultrasonic-Assisted Dispersive Magnetic Solid-Phase Extraction Method: Isotherm Adsorption. *Res. Chem. Intermed.* **2022**, *48*, 4269–4286. [CrossRef]
21. Mutalib, A.A.A.; Jaafar, N.F. Potential of Deep Eutectic Solvent in Photocatalyst Fabrication Methods for Water Pollutant Degradation: A Review. *J. Environ. Chem. Eng.* **2022**, *10*, 107422. [CrossRef]
22. Długosz, O. Natural Deep Eutectic Solvents in the Synthesis of Inorganic Nanoparticles. *Materials* **2023**, *16*, 627. [CrossRef]
23. Gontrani, L.; Donia, D.T.; Maria Bauer, E.; Tagliatesta, P.; Carbone, M. Novel Synthesis of Zinc Oxide Nanoparticles from Type IV Deep Eutectic Solvents. *Inorg. Chim. Acta* **2023**, *545*, 121268. [CrossRef]
24. Martins, G.; Gogola, J.L.; Budni, L.H.; Janegitz, B.C.; Marcolino-Junior, L.H.; Bergamini, M.F. 3D-Printed Electrode as a New Platform for Electrochemical Immunosensors for Virus Detection. *Anal. Chim. Acta* **2021**, *1147*, 30–37. [CrossRef] [PubMed]
25. Glowacki, M.J.; Cieslik, M.; Sawczak, M.; Koterwa, A.; Kaczmarzyk, I.; Jendrzejewski, R.; Szynkiewicz, L.; Ossowski, T.; Bogdanowicz, R.; Niedzialkowski, P.; et al. Helium-Assisted, Solvent-Free Electro-Activation of 3D Printed Conductive Carbon-Polylactide Electrodes by Pulsed Laser Ablation. *Appl. Surf. Sci.* **2021**, *556*, 149788. [CrossRef]
26. Talibawo, J.; Nyarige, J.S.; Kyesmen, P.I.; Cyulinyana, M.C.; Diale, M. The Behavior of Hydrothermally Synthesized Hematite Nanorods Prepared on Spin Coated Seed Layers. *Mater. Res. Express* **2022**, *9*, 026401. [CrossRef]
27. Abdelrahman, E.A.; Al-Farraj, E.S. Facile Synthesis and Characterizations of Mixed Metal Oxide Nanoparticles for the Efficient Photocatalytic Degradation of Rhodamine B and Congo Red Dyes. *Nanomaterials* **2022**, *12*, 3992. [CrossRef]
28. Ali, S.; Sikdar, S.; Basak, S.; Roy, D.; Dakua, V.K.; Adhikary, P.; Roy, M.N. High Visual Colorimetric Determination of F- Ions by Exploiting the Inhibition of Oxidase Mimicking Activity of FeMnO4@GQD Nanocomposite. *ChemistrySelect* **2022**, *7*, e202201186. [CrossRef]
29. Khamis, A.M.; Abbas, Z.; Azis, R.S.; Mensah, E.E.; Alhaji, I.A. Fabrication and Characterization of Fe2O3-OPEFB-PTFE Nanocomposites for Microwave Shielding Applications. *Polym. Eng. Sci.* **2022**, *62*, 3577–3588. [CrossRef]
30. Yamashita, T.; Hayes, P. Analysis of XPS Spectra of Fe^{2+} and Fe^{3+} Ions in Oxide Materials. *Appl. Surf. Sci.* **2008**, *254*, 2441–2449. [CrossRef]
31. Kwon, J.H.; Chaudhari, K.N.; Coy, E.; Seo, J.H.; Ahn, S.J.; Lee, Y.H.; Lee, S.; Cho, Y.C.; Choi, O.; Lee, K.S.; et al. Reversible Conversion Reactions of Mesoporous Iron Oxide with High Initial Coulombic Efficiency for Lithium-Ion Batteries. *ACS Sustain. Chem. Eng.* **2021**, *9*, 16627–16636. [CrossRef]
32. Mohite, S.V.; Kim, S.; Lee, C.; Bae, J.; Kim, Y. Z-Scheme Heterojunction Photocatalyst: Deep Eutectic Solvents-Assisted Synthesis of Cu2O Nanocluster Improved Hydrogen Production of TiO_2. *J. Alloys Compd.* **2022**, *928*, 167168. [CrossRef]
33. Šutka, A.; Šutka, A.; Vanags, M.; Spule, A.; Eglītis, R.; Vihodceva, S.; Šmits, K.; Tamm, A.; Mežule, L. Identifying Iron-Bearing Nanoparticle Precursor for Thermal Transformation into the Highly Active Hematite Photo-Fenton Catalyst. *Catalysts* **2020**, *10*, 778. [CrossRef]
34. Changotra, R.; Varshney, L.; Paul Guin, J.; Dhir, A. Performance of Hematite Particles as an Iron Source for the Degradation of Ornidazole in Photo-Fenton Process. *J. Sol-Gel Sci. Technol.* **2018**, *85*, 203–212. [CrossRef]
35. Zhou, X.; Lan, J.; Liu, G.; Deng, K.; Yang, Y.; Nie, G.; Yu, J.; Zhi, L. Facet-Mediated Photodegradation of Organic Dye over Hematite Architectures by Visible Light. *Angew. Chem. Int. Ed.* **2012**, *51*, 178–182. [CrossRef]
36. Liu, X.; Liu, J.; Chang, Z.; Sun, X.; Li, Y. Crystal Plane Effect of Fe_2O_3 with Various Morphologies on CO Catalytic Oxidation. *Catal. Commun.* **2011**, *12*, 530–534. [CrossRef]
37. Rojas-Mantilla, H.D.; Ayala-Duran, S.C.; Pupo Nogueira, R.F. Nontronite Mineral Clay NAu-2 as Support for Hematite Applied as Catalyst for Heterogeneous Photo-Fenton Processes. *Chemosphere* **2021**, *277*, 130258. [CrossRef] [PubMed]
38. Feng, X.; Luo, M.; Huang, W.; Huang, Y.; Xie, H.; Xu, Z.; Zhang, J.; Luo, W.; Wang, S.; Lin, H. The Degradation of BPA on Enhanced Heterogeneous Photo-Fenton System Using EDDS and Different Nanosized Hematite. *Environ. Sci. Pollut. Res.* **2020**, *27*, 23062–23072. [CrossRef]
39. Tatarchuk, T.; Danyliuk, N.; Lapchuk, I.; Macyk, W.; Shyichuk, A.; Kutsyk, R.; Kotsyubynsky, V.; Boichuk, V. Oxytetracycline Removal and E. Coli Inactivation by Decomposition of Hydrogen Peroxide in a Continuous Fixed Bed Reactor Using Heterogeneous Catalyst. *J. Mol. Liq.* **2022**, *366*, 120267. [CrossRef]
40. Domacena, A.M.G.; Aquino, C.L.E.; Balela, M.D.L. Photo-Fenton Degradation of Methyl Orange Using Hematite (α-Fe_2O_3) of Various Morphologies. *Mater. Today Proc.* **2020**, *22*, 248–254. [CrossRef]
41. Ali, A.S.; Khan, I.; Zhang, B.; Nomura, K.; Homonnay, Z.; Kuzmann, E.; Scrimshire, A.; Bingham, P.A.; Krehula, S.; Musić, S.; et al. Photo-Fenton Degradation of Methylene Blue Using Hematite-Enriched Slag under Visible Light. *J. Radioanal. Nucl. Chem.* **2020**, *325*, 537–549. [CrossRef]
42. Navalon, S.; Alvaro, M.; Garcia, H. Heterogeneous Fenton Catalysts Based on Clays, Silicas and Zeolites. *Appl. Catal. B Environ.* **2010**, *99*, 1–26. [CrossRef]
43. Rosales, E.; Anasie, D.; Pazos, M.; Lazar, I.; Sanromán, M.A. Kaolinite Adsorption-Regeneration System for Dyestuff Treatment by Fenton Based Processes. *Sci. Total Environ.* **2018**, *622–623*, 556–562. [CrossRef] [PubMed]
44. Acevedo-García, V.; Rosales, E.; Puga, A.; Pazos, M.; Sanromán, M.A. Synthesis and Use of Efficient Adsorbents under the Principles of Circular Economy: Waste Valorisation and Electroadvanced Oxidation Process Regeneration. *Sep. Purif. Technol.* **2020**, *242*, 116796. [CrossRef]

45. Niveditha, S.V.; Gandhimathi, R. Flyash Augmented Fe3O4 as a Heterogeneous Catalyst for Degradation of Stabilized Landfill Leachate in Fenton Process. *Chemosphere* **2020**, *242*, 125189. [CrossRef]
46. Ma, C.; He, Z.; Jia, S.; Zhang, X.; Hou, S. Treatment of Stabilized Landfill Leachate by Fenton-like Process Using Fe 3 O 4 Particles Decorated Zr-Pillared Bentonite. *Ecotoxicol. Environ. Saf.* **2018**, *161*, 489–496. [CrossRef]
47. Ghasemi, H.; Aghabarari, B.; Alizadeh, M.; Khanlarkhani, A.; Abu-Zahra, N. High Efficiency Decolorization of Wastewater by Fenton Catalyst: Magnetic Iron-Copper Hybrid Oxides. *J. Water Process Eng.* **2020**, *37*, 101540. [CrossRef]
48. Ushani, U.; Lu, X.; Wang, J.; Zhang, Z.; Dai, J.; Tan, Y.; Wang, S.; Li, W.; Niu, C.; Cai, T.; et al. Sulfate Radicals-Based Advanced Oxidation Technology in Various Environmental Remediation: A State-of-the–Art Review. *Chem. Eng. J.* **2020**, *402*, 126232. [CrossRef]
49. Xu, H.; Wang, D.; Ma, J.; Zhang, T.; Lu, X.; Chen, Z. A Superior Active and Stable Spinel Sulfide for Catalytic Peroxymonosulfate Oxidation of Bisphenol S. *Appl. Catal. B Environ.* **2018**, *238*, 557–567. [CrossRef]
50. Wu, Z.; Xiong, Z.; Liu, R.; He, C.; Liu, Y.; Pan, Z.; Yao, G.; Lai, B. Pivotal Roles of N-Doped Carbon Shell and Hollow Structure in Nanoreactor with Spatial Confined Co Species in Peroxymonosulfate Activation: Obstructing Metal Leaching and Enhancing Catalytic Stability. *J. Hazard. Mater.* **2022**, *427*, 128204. [CrossRef]
51. Wang, G.; Chen, S.; Quan, X.; Yu, H.; Zhang, Y. Enhanced Activation of Peroxymonosulfate by Nitrogen Doped Porous Carbon for Effective Removal of Organic Pollutants. *Carbon N. Y.* **2017**, *115*, 730–739. [CrossRef]
52. Yang, S.; Xu, S.; Tong, J.; Ding, D.; Wang, G.; Chen, R.; Jin, P.; Wang, X.C. Overlooked Role of Nitrogen Dopant in Carbon Catalysts for Peroxymonosulfate Activation: Intrinsic Defects or Extrinsic Defects? *Appl. Catal. B Environ.* **2021**, *295*, 120291. [CrossRef]
53. Xu, J.; Song, J.; Min, Y.; Xu, Q.; Shi, P. Mg-Induced g-C_3N_4 Synthesis of Nitrogen-Doped Graphitic Carbon for Effective Activation of Peroxymonosulfate to Degrade Organic Contaminants. *Chin. Chem. Lett.* **2022**, *33*, 3113–3118. [CrossRef]
54. Wang, S.; Xu, L.; Wang, J. Nitrogen-Doped Graphene as Peroxymonosulfate Activator and Electron Transfer Mediator for the Enhanced Degradation of Sulfamethoxazole. *Chem. Eng. J.* **2019**, *375*, 122041. [CrossRef]
55. Fan, J.; Gu, L.; Wu, D.; Liu, Z. Mackinawite (FeS) Activation of Persulfate for the Degradation of p-Chloroaniline: Surface Reaction Mechanism and Sulfur-Mediated Cycling of Iron Species. *Chem. Eng. J.* **2018**, *333*, 657–664. [CrossRef]
56. Zhang, X.; Deng, H.; Zhang, G.; Yang, F.; Yuan, G.E. Natural Bornite as an Efficient and Cost-Effective Persulfate Activator for Degradation of Tetracycline: Performance and Mechanism. *Chem. Eng. J.* **2020**, *381*, 122717. [CrossRef]
57. Long, Y.; Li, S.; Su, Y.; Wang, S.; Zhao, S.; Wang, S.; Zhang, Z.; Huang, W.; Liu, Y.; Zhang, Z. Sulfur-Containing Iron Nanocomposites Confined in S/N Co-Doped Carbon for Catalytic Peroxymonosulfate Oxidation of Organic Pollutants: Low Iron Leaching, Degradation Mechanism and Intermediates. *Chem. Eng. J.* **2021**, *404*, 126499. [CrossRef]
58. Dong, L.; Xu, T.; Chen, W.; Lu, W. Synergistic Multiple Active Species for the Photocatalytic Degradation of Contaminants by Imidazole-Modified g-C3N4 Coordination with Iron Phthalocyanine in the Presence of Peroxymonosulfate. *Chem. Eng. J.* **2019**, *357*, 198–208. [CrossRef]
59. Wang, Z.; Wang, Z.; Li, W.; Lan, Y.; Chen, C. Performance Comparison and Mechanism Investigation of Co_3O_4-Modified Different Crystallographic MnO_2 (α, β, γ, and δ) as an Activator of Peroxymonosulfate (PMS) for Sulfisoxazole Degradation. *Chem. Eng. J.* **2022**, *427*, 130888. [CrossRef]
60. Fan, S.; Shang, J.; Kulan, S.; He, X.; Wang, X.; Nasen, B.; Nie, J.; Feng, D.; Cheng, X. Enhanced Degradation of Carbamazepine in Water over SC-Modified $NiFe_2S_4$ Nanocomposites by Peroxymonosulfate Activation. *Chem. Eng. J.* **2022**, *450*, 138190. [CrossRef]
61. Poza-Nogueiras, V.; Rosales, E.; Pazos, M.; Sanromán, M.Á. Current Advances and Trends in Electro-Fenton Process Using Heterogeneous Catalysts—A Review. *Chemosphere* **2018**, *201*, 399–416. [CrossRef] [PubMed]
62. Yao, Y.; Pan, Y.; Yu, Y.; Yu, Z.; Lai, L.; Liu, F.; Wei, L.; Chen, Y. Bifunctional Catalysts for Heterogeneous Electro-Fenton Processes: A Review. *Environ. Chem. Lett.* **2022**, *20*, 3837–3859. [CrossRef]
63. Panizza, M.; Cerisola, G. Electro-Fenton Degradation of Synthetic Dyes. *Water Res.* **2009**, *43*, 339–344. [CrossRef] [PubMed]
64. Wang, M.; Kang, J.; Li, S.; Zhang, J.; Tang, Y.; Liu, S.; Liu, J.; Tang, P. Electro-Assisted Heterogeneous Activation of Peroxymonosulfate by g-C3N4 under Visible Light Irradiation for Tetracycline Degradation and Its Mechanism. *Chem. Eng. J.* **2022**, *436*, 135278. [CrossRef]
65. Bai, C.; Yang, G.; Zhang, S.; Deng, S.; Zhang, Y.; Chen, C.; He, J.; Xu, M.; Long, L. A Synergistic System of Electrocatalytic-Anode/α-MnO_2/Peroxymonosulfate for Removing Combined Pollution of Tetracycline and Cr(VI). *Chem. Eng. J.* **2021**, *423*, 130284. [CrossRef]
66. Long, X.; Xiong, Z.; Huang, R.; Yu, Y.; Zhou, P.; Zhang, H.; Yao, G.; Lai, B. Sustainable Fe(III)/Fe(II) Cycles Triggered by Co-Catalyst of Weak Electrical Current in Fe(III)/Peroxymonosulfate System: Collaboration of Radical and Non-Radical Mechanisms. *Appl. Catal. B Environ.* **2022**, *317*, 121716. [CrossRef]
67. Xiao, R.; Luo, Z.; Wei, Z.; Luo, S.; Spinney, R.; Yang, W.; Dionysiou, D.D. Activation of Peroxymonosulfate/Persulfate by Nanomaterials for Sulfate Radical-Based Advanced Oxidation Technologies. *Curr. Opin. Chem. Eng.* **2018**, *19*, 51–58. [CrossRef]
68. Gong, F.; Wang, L.; Li, D.; Zhou, F.; Yao, Y.; Lu, W.; Huang, S.; Chen, W. An Effective Heterogeneous Iron-Based Catalyst to Activate Peroxymonosulfate for Organic Contaminants Removal. *Chem. Eng. J.* **2015**, *267*, 102–110. [CrossRef]
69. Bararpour, S.T.; Feylizadeh, M.R.; Delparish, A.; Qanbarzadeh, M.; Raeiszadeh, M.; Feilizadeh, M. Investigation of 2-Nitrophenol Solar Degradation in the Simultaneous Presence of $K_2S_2O_8$ and H_2O_2: Using Experimental Design and Artificial Neural Network. *J. Clean. Prod.* **2018**, *176*, 1154–1162. [CrossRef]

70. Guan, Y.-H.; Ma, J.; Ren, Y.-M.; Liu, Y.-L.; Xiao, J.-Y.; Lin, L.-Q.; Zhang, C. Efficient Degradation of Atrazine by Magnetic Porous Copper Ferrite Catalyzed Peroxymonosulfate Oxidation via the Formation of Hydroxyl and Sulfate Radicals. *Water Res.* **2013**, *47*, 5431–5438. [CrossRef]
71. Giannakis, S.; Lin, K.Y.A.; Ghanbari, F. A Review of the Recent Advances on the Treatment of Industrial Wastewaters by Sulfate Radical-Based Advanced Oxidation Processes (SR-AOPs). *Chem. Eng. J.* **2021**, *406*, 127083. [CrossRef]
72. Scaria, J.; Nidheesh, P.V. Comparison of Hydroxyl-Radical-Based Advanced Oxidation Processes with Sulfate Radical-Based Advanced Oxidation Processes. *Curr. Opin. Chem. Eng.* **2022**, *36*, 100830. [CrossRef]
73. Nguyen, N.T.T.; Nguyen, A.Q.K.; Kim, M.S.; Lee, C.; Kim, S.; Kim, J. Degradation of Aqueous Organic Pollutants Using an Fe2O3/WO3 Composite Photocatalyst as a Magnetically Separable Peroxymonosulfate Activator. *Sep. Purif. Technol.* **2021**, *267*, 118610. [CrossRef]
74. Sheikhi, S.; Jebalbarezi, B.; Dehghanzadeh, R.; Maryamabadi, A.; Aslani, H. Sulfamethoxazole Oxidation in Secondary Treated Effluent Using Fe(VI)/PMS and Fe(VI)/H2O2processes: Experimental Parameters, Transformation Products, Reaction Pathways and Toxicity Evaluation. *J. Environ. Chem. Eng.* **2022**, *10*, 107446. [CrossRef]
75. Martini, J.; Orge, C.A.; Faria, J.L.; Pereira, M.F.R.; Soares, O.S.G.P. Catalytic Advanced Oxidation Processes for Sulfamethoxazole Degradation. *Appl. Sci.* **2019**, *9*, 2652. [CrossRef]
76. Puga, A.; Rosales, E.; Sanromán, M.A.; Pazos, M. Environmental Application of Monolithic Carbonaceous Aerogels for the Removal of Emerging Pollutants. *Chemosphere* **2020**, *248*, 125995. [CrossRef] [PubMed]
77. Priac, A.; Badot, P.M.; Crini, G. Évaluation de La Phytotoxicité d'eaux de Rejets via Lactuca Sativa: Paramètres Des Tests de Germination et d'élongation. *Comptes Rendus Biol.* **2017**, *340*, 188–194. [CrossRef] [PubMed]
78. Sakthi Sri, S.P.; Taj, J.; George, M. Facile Synthesis of Magnetite Nanocubes Using Deep Eutectic Solvent: An Insight to Anticancer and Photo-Fenton Efficacy. *Surf. Interfaces* **2020**, *20*, 100609. [CrossRef]